JMEPEG (2015) 24:1237–1242
DOI: 10.1007/s11665-015-1399-z

1059-9495/$19.00

Synthesis and Evaluation of Fluorescent Magnetic Composites as Targeted Drug Delivery Carriers

Wei Jiang, Xiaolong Chen, Juan Wu, Shanshan Xu, and Renbing Tian

(Submitted September 23, 2014; in revised form December 4, 2014; published online January 27, 2015)

We have developed Fe_3O_4@ZnS-based fluorescent magnetic composites as targeted drug delivery carriers via a facile route. The results indicated that the composites exhibited both magnetic and fluorescent properties. Fe_3O_4@ZnS possessed high saturation magnetization (68.25 emu/g) at room temperature. Ultraviolet light can be easily obtained by exposing the microspheres to different excitation wavelengths. The drug loading studies showed that Fe_3O_4@ZnS-based fluorescent magnetic composites had an excellent drug loading performance. These traits made the composites better for the application of medical imaging and magnetic targeted drug delivery.

Keywords drug delivery, Fe_3O_4, fluorescence, magnetic targeted

1. Introduction

With the progresses of medical technology, biomaterials with single function cannot meet the needs of experimental research and clinic usage in the field of tumor therapy. Superparamagnetic iron oxide nanoparticles have been investigated extensively for biomedical applications such as tumor-specific targeted (Ref 1, 2), gene therapy (Ref 3), protein therapy (Ref 4), drug delivery (Ref 5, 6), and so on. Regrettably, magnetic nanoparticles have no function of marking. Therefore, magnetic particles that are modified by substances with fluorescently labeled function have attracted wide attention of researchers (Ref 7, 8).

However, fluorescent substances, whose main limitation is that when combined with other materials, it will produce quenching phenomenon due to the effect of free radicals or inappropriate ligand. In order to prevent the quenching phenomenon, the magnetic particles should be coated with protective layer. SiO_2 has been exploited as the most popular coating material for magnetic nanoparticles (Ref 9, 10). Silica has several advantages as firstly, it may provide both chemical and physical shielding from the direct environment to improve the stability; secondly, it can reduce the release of cytotoxic ions and prevent photooxidation (Ref 11-13); thirdly, Fe_3O_4@-SiO_2 facilitates the hydrophilicity of Fe_3O_4 and allow the composite particles for further use (Ref 14-16). However, the SiO_2 layer could directly lead to the increase of nanoparticles' size and also affect their magnetism. Moreover, during the preparation process of Fe_3O_4@SiO_2, different silane coupling agents are required to be used, and the synthetic procedure is rather complex and time consuming.

Wei Jiang, Xiaolong Chen, Juan Wu, Shanshan Xu, and **RenbingTian,** National Special Superfine Powder Engineering Research Center, Nanjing University of Science and Technology, Nanjing 210094, China. Contact e-mail: superfine_jw@126.com.

All the fluorescence substances, II-VI group semiconductor quantum dots have gained considerable attention in the past decade (Ref 17-20). Zinc sulfide, as a unique II-VI group semiconductor of direct transition type, has been used in the fabrication of solar cells (Ref 21), LED (Ref 22), electroluminescent displays (Ref 23), and so on. Zinc sulfide owns some excellent advantages: (1) strong luminescent properties, (2) environmental adaptability, (3) ease of synthesis, (4) low raw material prices, and (5) as a coating material without the disadvantages of silane coupling agents.

Herein, following the above principles, for combining the characteristics of magnetism with biological markedness, we developed a facile route to synthesize trifunctional composite for drug delivery (Scheme 1). The synthesized composites were characterized by x-ray diffraction (XRD), transmission electron microscopy (TEM), Fourier transform infrared spectroscopy (FT-IR), vibrating sample magnetometer (VSM), and fluorescence emission (FL) spectra. The drug loading performance was studied using bull serum albumin (BSA) and doxorubicin (DOX).

2. Experimental

2.1 Materials

All chemicals were analytical grade and used without further purification. Ferric chloride ($FeCl_3{\cdot}6H_2O$), Zinc acetate ($Zn(Ac)_2$), citric acid (CA), and polyethylene glycol (PEG-4000) were purchased from Sinopharm Chemical Reagent Co. Ltd., Shanghai, China. Thioacetamide (TAA) was supplied by Aladdin. BSA was purchased from Shanghai Huixing Biochemical Reagent Co., Ltd., Shanghai, China. DOX was purchased from Yuanye Biotechnology Co. Ltd., Shanghai, China. All other chemicals and solvents used in this study were of high analytical grade and commercially available.

2.2 Synthesis of Fe_3O_4 Particles

The Fe_3O_4 particles were synthesized by solvothermal method (Ref 24). Typically, $FeCl_3{\cdot}6H_2O$ (1.35 g), carbamide (3.60 g), and PEG-4000 (4.00 g) were dissolved in 40 mL EG, the mixture was stirred vigorously to ensure all materials

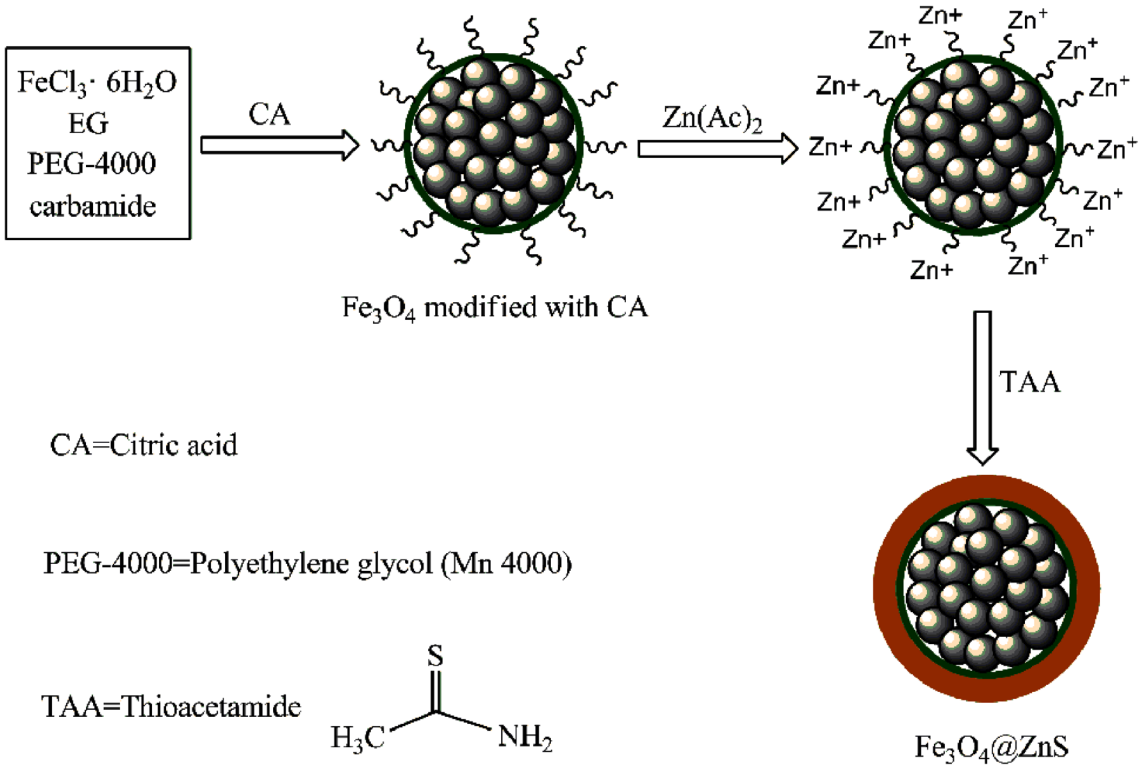

Scheme 1 Schematic representation of the formation of fluorescent magnetic composites

dissolve completely. Then, the mixture was transferred to a Teflon-lined stainless-steel autoclave and sealed for heating at 200 °C for 8 h. The precipitated black products were collected from the solution with an external magnet and washed with ethanol and water for several times.

2.3 Fabrication of Fe_3O_4@ZnS with Core-Shell Structure

In order to avoid the quenching phenomenon, CA was used as partition to modified Fe_3O_4 particles (Ref 25). Briefly, 8.0 g CA was added to 100 mL suspension of Fe_3O_4, and then the reaction was continued for 4 h under stirring and ultrasound at room temperature. The colloidal Fe_3O_4 was separated by magnetic decantation and washed with ethanol and water. Finally, the biocompatible Fe_3O_4 particles were dispersed in 100 mL isopropanol to form a magnetic fluid (MF). Then, 2.0 g $Zn(Ac)_2$ was dissolved in 60 mL isopropanol, and 5 mL MF was dropwise added under ultrasound and mechanical stirring for 30 min, and the reaction was continued for 24 h. After that, 60 mL TAA (1.0 g) aqueous solution was added slowly under N_2 atmosphere at 65 °C and reacted for 6 h. Finally, the products were collected and washed with water for several times to separate the otiose ZnS. The final products were dried under vacuum at 60 °C.

2.4 Drug Loading Studies

As shown in Fig. 1, the dry Fe_3O_4@ZnS particles were dispersed in 100 mL deionized water, 1.0 g BSA was added under stirring and ultrasound for 10 min. Then the BSA-coated Fe_3O_4@ZnS was collected by a magnet, washed with water, and dried under vacuum. After that, 10 mg dry BSA-coated Fe_3O_4@ZnS was dispersed into 100 mL DOX solutions which were prepared in advance at different concentrations. After stirring and ultrasound for 5 min, particles were collected by a magnet, the solutions were analyzed by ultraviolet-visible (UV-Vis) at 482 nm to determine the loading capacity and encapsulation efficiency of BSA-coated Fe_3O_4@ZnS.

2.5 Characterizations

The morphology of composites was observed by transmission electron microscopy (TEM, Model Tecnai 12, Philips Co. Ltd., Holland). FT-IR spectroscopies were measured on a Vector22 spectrometer (Bruker Co. Ltd., Germany). Furthermore, X-ray diffractometer (XRD, D/max 18 kV, Bruker D8 Super Speed) with Cu K_α radiation was used to ensure the crystalline phase, and the magnetic properties of the samples were measured using a vibrating sample magnetometer (VSM, Model7410, Lake Shore Co. Ltd., USA) at room temperature. The FL spectra were recorded by a Hitachi F-4500 fluorescence spectrophotometer with a Xe lamp as the excitation source (Tokyo, Japan).

3. Results and Discussion

In Fig. 2, the diffraction peaks with 2θ values of 30°, 35°, 43°, 53°, 57°, and 63° correspond to the (220), (311), (400), (422), (511), and (440) reflection planes of magnetite Fe_3O_4, respectively (JCPDS No. 19-0629). The diffraction peaks with 2θ values of 27°, 47°, and 61° correspond to the (002), (110), and (202) reflection planes of wurtzite ZnS (JCPDS No. 12-0688). These revealed that ZnS shell formed onto Fe_3O_4 and Fe_3O_4 particles was stable during the coating process.

Figure 3(a) shows the microscopy of Fe_3O_4 nanoparticles modified with CA, and the mean size is about 200 nm.

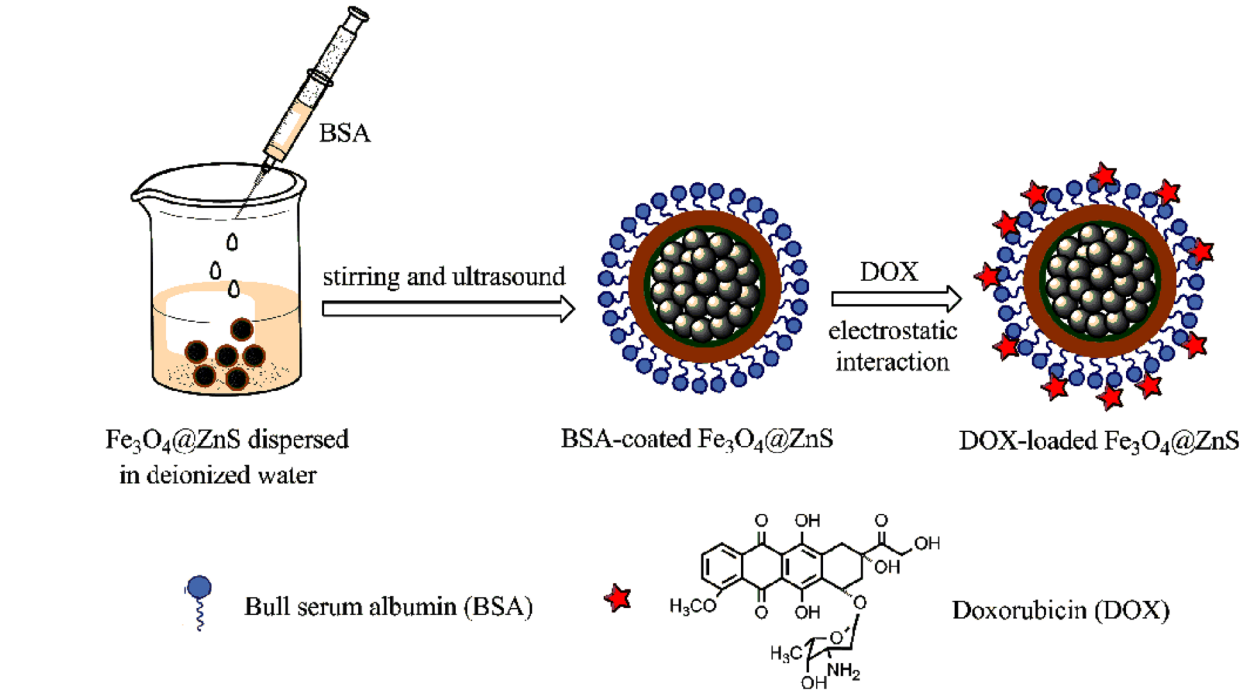

Fig. 1 Mechanism of magnetic fluorescent composite microspheres loaded with drug

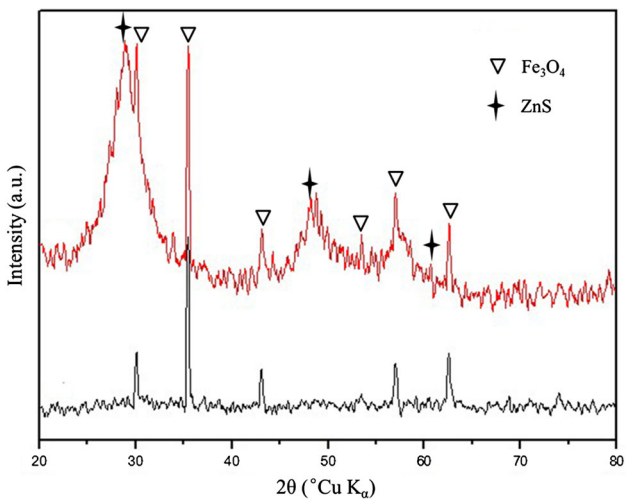

Fig. 2 X-ray diffraction (XRD) patterns of (a) as-synthesized Fe_3O_4 microspheres and (b) Fe_3O_4@ZnS microspheres

Figure 3(b-d) clearly reveals that the Fe_3O_4 core was coated with ZnS shell. The thickness of ZnS shell in the core-shell structure gradually changed with different inverse proportion of Fe_3O_4 and ZnS. Overall ratios, the most appropriate is 1:1 according to Fig. 3(c).

Figure 4 shows the FT-IR analysis of Fe_3O_4 modified with CA and Fe_3O_4@ZnS. The absorption bands around 3400 cm^{-1} correspond to the stretching vibration of -OH. The FT-IR bands at low wavenumbers (590 cm^{-1}) were consistent with the characteristic absorption of Fe-O. The peaks at 1130 and 1398 cm^{-1} attribute to the C-O stretching vibration of primary alcohol and carboxyl, respectively. The shoulder at 1624 cm^{-1} is assigned to the C=O of CA. These three peaks strongly confirmed the presence of citric acid on the surface of Fe_3O_4.

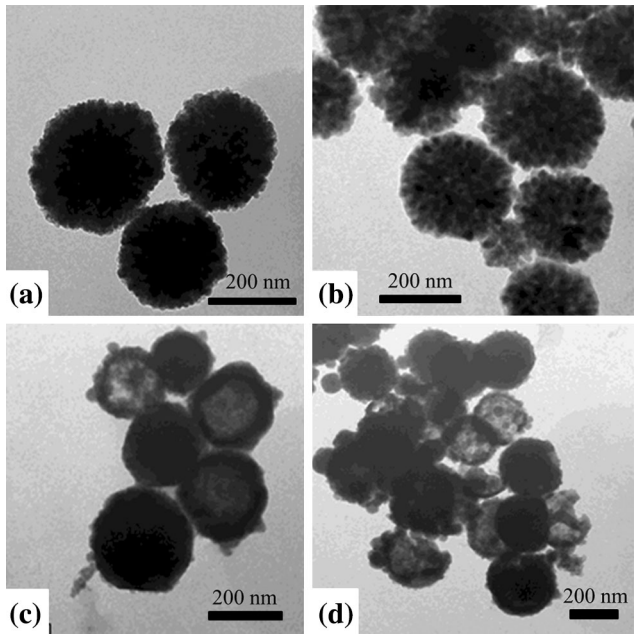

Fig. 3 Transmission electron microscopy (TEM) micrographs of (a) Fe_3O_4 nanoparticles modified with CA, Fe_3O_4@ZnS with different proportions of Fe:Zn (b) 1:3, (c) 1:1, (d) 1:2

Figure 5 shows that the saturation magnetization (M_s) value of Fe_3O_4 is 85.9 emu/g, corresponding to the value reported before (Ref 26). After being modified with ZnS, the M_s value decreased to 68.2 emu/g. In addition, no evident hysteresis loops can be observed, these revealed that Fe_3O_4 and Fe_3O_4@ZnS microspheres are all superparamagnetic at room temperature, which further confirmed the application of Fe_3O_4@ZnS in the area of targeted drug delivery.

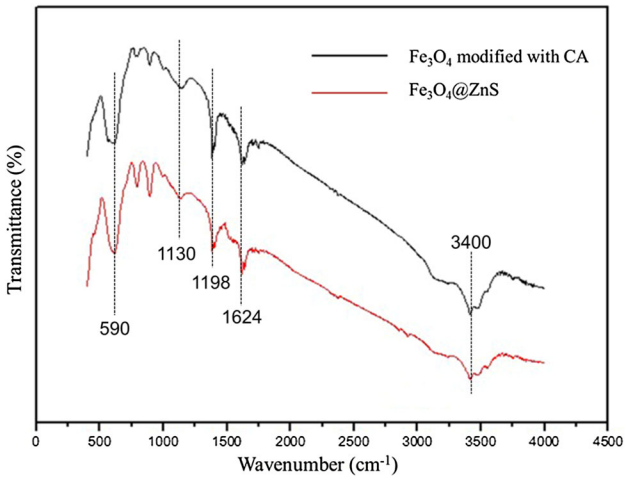

Fig. 4 Fourier transform infrared (FT-IR) spectras of (a) Fe_3O_4 modified with CA and (b) Fe_3O_4@ZnS

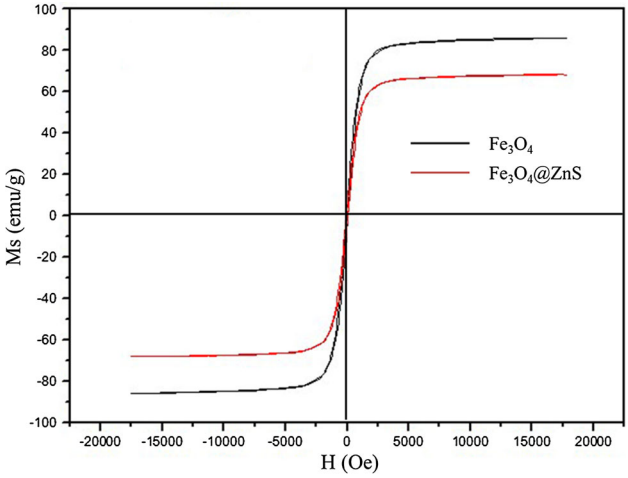

Fig. 5 Vibrating sample magnetometer (VSM) measurement results of (a) Fe_3O_4 and (b) Fe_3O_4@ZnS

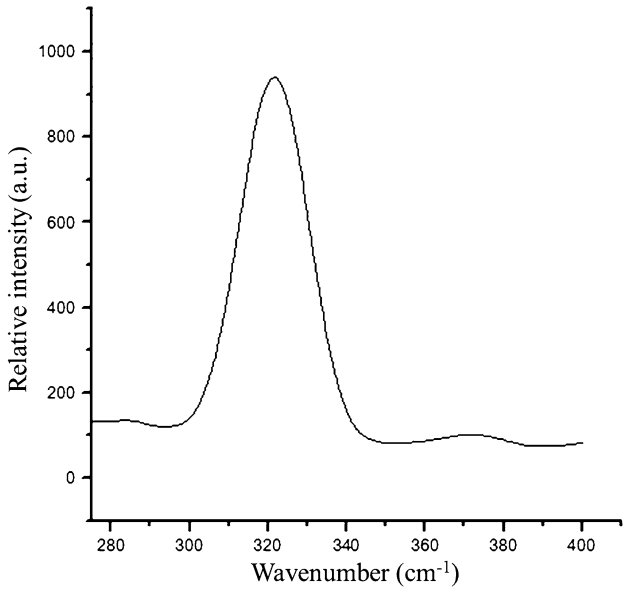

Fig. 6 The fluorescence emission (FL) spectra of Fe_3O_4@ZnS excited at 225 nm at room temperature

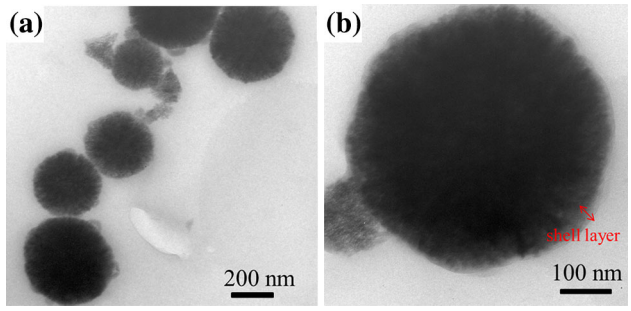

Fig. 7 Transmission electron microscopy (TEM) micrograph of BSA-coated composite particles. (a) the whole and (b) the single

In the process of combining magnetic particles and quantum dots, the most important problem is to prevent the quenching of quantum dots. Figure 6 shows the photoluminescence (PL) spectra of Fe_3O_4@ZnS microspheres, the main emission peak at 323.3 nm excited by Xe light at 225 nm, corresponding to the intrinsic band gap emission of bulk wurtzite ZnS (Ref 27). It indicates that the composite particles did not result in quenching of the quantum dots, which is very important for the application in medical imaging. On the basis of the above discussions, Fe_3O_4/ZnS possesses properties of both fluorescence and magnetism, and may serve as targeted and tracing drug delivery carrier in tumor treatment.

Figure 7 shows the morphology of BSA-coated Fe_3O_4@ZnS. After coating with BSA, a thin layer formed onto the surface of Fe_3O_4@ZnS, and the morphology of the microspheres appeared to be more spherical. Figure 8 shows the effects of DOX concentration on drug loading capacity and encapsulation efficiency of BSA-coated Fe_3O_4@ZnS.

In Fig. 8, with the initial concentration of DOX increased, the drug loading capacity also increased, when the concentration of DOX was more than 35 mg/L, the drug absorption started to level off with little change in drug loading capacity, indicating that the drug loading was gradually saturated. In contrast, the drug encapsulation efficiency had been reduced with the increase of the initial concentration of DOX. The highest encapsulation efficiency was 67.3% at the concentration of 5 mg/L. When the concentration of DOX was more than 15 mg/L, the encapsulation efficiency reduced rapidly. Therefore, the optimal initial drug concentration was about 15 mg/L. At this point, the drug loading capacity and encapsulation efficiency can achieve the best with each other. All of these revealed that BSA-coated Fe_3O_4@ZnS could be used as drug delivery carriers and Fe_3O_4@ZnS may have the potential to be used as multifunctional drug delivery carriers in the field of targeted cancer therapy.

4. Conclusion

In summary, Fe_3O_4@ZnS composites have been synthesized via a facile route, and the products exhibit fluorescence, display

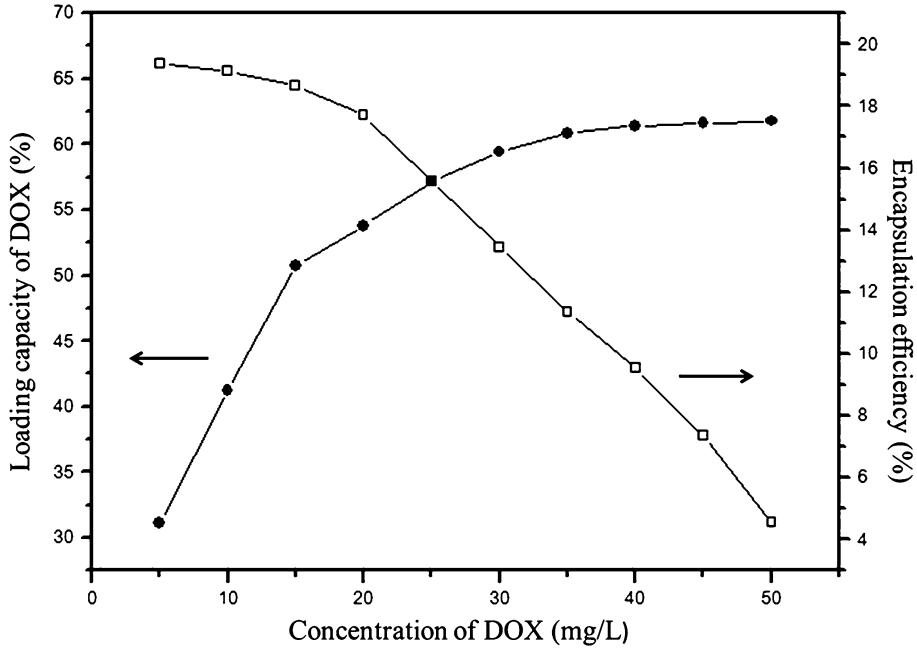

Fig. 8 The effects of initial DXR concentrations on the drug loading capacity and encapsulation efficiency of BSA-coated composite particles

excellent magnetic properties at room temperature. From the drug loading studies, BSA can be successfully coated onto Fe_3O_4@ZnS, and the BSA-coated Fe_3O_4@ZnS microspheres have excellent drug loading performance. Thus, the bifunctional magnetic optical Fe_3O_4@ZnS microspheres may have great potential applications in tracking targeted drug delivery. And this facile synthetic procedure may be widely applicable in the synthesis of multifunctional composites with core-shell hetero-structures using different cation or anion surfactants.

Acknowledgments

The authors are grateful for National Science Foundation of China (Project Nos. 50602024, 50972060), the Scientific and Technical Supporting Programs of Jiangsu Province (BE2012758), the Scientific Research Fund from NJUST Research Funding (No. 2010ZDJH06), the Fundamental Research Funds for the Central Universities (No. 30920130112003), and a Project Funded by the Priority Academic Program Development of Jiangsu Higher Education Institutions.

References

1. R. Sharma and S. Kwon, New Applications of Nanoparticles in Cardiovascular Imaging, *J. Exp. Nanosci.*, 2007, **2**, p 115–126
2. F.M. Kievit and M.Q. Zhang, Surface Engineering of Iron Oxide Nanoparticles for Targeted Cancer Therapy, *Acc. Chem. Res.*, 2011, **44**, p 853–862
3. C. Dempsey, I. Lee, K.R. Cowan, and J. Suh, Coating Barium Titanate Nanoparticles with Polyethylenimine Improves Cellular Uptake and Allows for Coupled Imaging and Gene Delivery, *Colloids Surf. B*, 2013, **112**, p 108–112
4. I.C. Masthoff, F. David, C. Wittmann, and G. Garnweitner, Functionalization of Magnetic Nanoparticles with High-Binding Capacity for Affinity Separation of Therapeutic Proteins, *J. Nanopart. Res.*, 2014, **16**, p 2164
5. A. Arizaga, G. Ibarz, R. Pinol, and A. Urtizberea, Encapsulation of Magnetic Nanoparticles in a pH-Sensitive Poly(4-vinyl pyridine) Polymer: A Step Forward to a Multi-responsive System, *J. Exp. Nanosci.*, 2014, **9**, p 561–569
6. W.C. She, N. Li, K. Luo, C.H. Guo, G. Wang, Y.Y. Geng, and Z.W. Gu, Dendronized Heparin-Doxorubicin Conjugate Based Nanoparticle as pH-Responsive Drug Delivery System for Cancer Therapy, *Biomaterials*, 2013, **34**, p 2252–2264
7. Y.S. Lin, C.P. Tsai, H.Y. Huang, C.T. Kuo, Y. Hung, D.M. Huang, Y.C. Chen, and C.Y. Mou, Well-Ordered Mesoporous Silica Nanoparticles as Cell Markers, *Chem. Mater.*, 2005, **17**, p 4570–4573
8. K. Vuu, J.W. Xie, M.A. McDonald, M. Bernardo, F. Hunter, Y.T. Zhang, K. Li, M. Bednarski, and S. Guccione, Gadolinium-Rhodamine Nanoparticles for Cell Labeling and Tracking via Magnetic Resonance and Optical Imaging, *Bioconjug. Chem.*, 2005, **16**, p 995–999
9. K. Woo, J. Hong, and J.P. Ahn, Synthesis and Surface Modification of Hydrophobic Magnetite to Processible Magnetite@Silica-Propylamine, *J. Magn. Magn. Mater.*, 2005, **293**, p 177–181
10. I.J. Bruce, J. Taylor, M. Todd, M.J. Davies, E. Borioni, C. Sangregorio, and T. Sen, Synthesis, Characterisation and Application of Silica-Magnetite Nanocomposites, *J. Magn. Magn. Mater.*, 2004, **284**, p 145–160
11. S.T. Selvan, T.T. Tan, and J.Y. Ying, Robust, Non-cytotoxic, Silica-Coated CdSe Quantum Dots with Efficient Photoluminescence, *Adv. Mater.*, 2005, **17**, p 1620–1625
12. T.T. Zhang, J.L. Stilwell, D. Gerion, L.H. Ding, O. Elboudwarej, P.A. Cooke, J.W. Gray, A.P. Alivisatos, and F.F. Chen, Cellular Effect of High Doses of Silica-Coated Quantum Dot Profiled with High Throughput Gene Expression Analysis and High Content Cellomics Measurements, *Nano Lett.*, 2005, **6**, p 800–808
13. C. Kirchner, T. Liedl, S. Kudera, T. Pellegrino, A.M. Javier, H.E. Gaub, S. Stolzle, N. Fertig, and W.J. Parak, Cytotoxicity of Colloidal CdSe and CdSe/ZnS Nanoparticles, *Nano Lett.*, 2005, **5**, p 331–338
14. Y.H. Yang, L.H. Jing, X.L. Yu, D.D. Yan, and M.Y. Gao, Coating Aqueous Quantum Dots with Silica via Reverse Microemulsion Method: Toward Size-Controllable and Robust Fluorescent Nanoparticles, *Chem. Mater.*, 2007, **19**, p 4123–4128
15. F.Q. Chen and D. Gerion, Fluorescent CdSe/ZnS Nanocrystal-Peptide Conjugates for Long-Term, Nontoxic Imaging and Nuclear Targeting in Living Cells, *Nano Lett.*, 2004, **4**, p 1827–1832
16. J.H. Lee, Y.W. Jun, S.I. Yeon, J.S. Shin, and J. Cheon, Dual-Mode Nanoparticle Probes for High-Performance Magnetic Resonance and

Fluorescence Imaging of Neuroblastoma, *Angew. Chem. Int. Ed.*, 2006, **45**, p 8160–8162

17. M. Feng and H.B. Zhan, CdS Nanobubbles and Cd-DMS Nanosheets: Solvothermal Synthesis and Formation Mechanism, *J. Nanosci. Nanotechnol.*, 2013, **13**, p 924–928
18. G.N. Wang, C. Wang, Q. Ma, and X.G. Su, Synthesis of Dual Fluorescent Encoding Magnetic Composite Nanoparticles, *J. Nanosci. Nanotechnol.*, 2010, **10**, p 1956–1963
19. K.S. Choi, B.K. Bang, P.K. Bae, Y.-R. Kim, and C.H. Kim, Synthesis of Fe_3O_4-ZnS/$AgInS_2$ Composite Nanoparticles Using a Hydrophobic Interaction, *J. Nanosci. Nanotechnol.*, 2013, **13**, p 1820–1823
20. G.H. Du, Z.L. Liu, D. Wang, X. Xia, L.H. Jia, K.L. Yao, Q. Chu, and S.M. Zhang, Characterization of Magnetic Fluorescence Fe_3O_4/CdSe Nanocomposites, *J. Nanosci. Nanotechnol.*, 2009, **9**, p 1304–1307
21. S.W. Shin, S.R. Kang, K.V. Gurav, J.H. Yun, J.-H. Moon, J.Y. Lee, and J.H. Kim, A Study on the Improved Growth Rate and Morphology of Chemically Deposited ZnS Thin Film Buffer Layer for Thin Film Solar Cells in Acidic Medium, *Sol. Energy*, 2011, **85**, p 2903–2911
22. N.H. Tuan, K.H. Koh, P.T. Nga, and S. Lee, Effect of Cathodes on High Efficiency Inorganic-Organic Hybrid LEDs Based on CdSe/ZnS Quantum Dots, *J. Cryst. Growth*, 2011, **326**, p 109–112
23. D.C. Koutsogeorgis, E.A. Mastio, W.M. Cranton, and C.B. Thomas, Pulsed KrF Laser Annealing of ZnS:Mn Laterally Emitting Thin Film Electroluminescent Displays, *Thin Solid Films*, 2001, **383**, p 31–33
24. H. Deng, X.L. Li, Q. Peng, X. Wang, J.P. Chen, and Y.D. Li, Monodisperse Magnetic Single-Crystal Ferrite Microspheres, *Angew. Chem. Int. Ed. Engl.*, 2005, **44**, p 2782–2785
25. Y.K. Sun, L. Duan, Z.R. Guo, D.M. Yun, M. Ma, L. Xu, Y. Zhang, and N. Gu, An Improved Way to Prepare Superparamagnetic Magnetite-Silica Core-Shell Nanoparticles for Possible Biological Application, *J. Magn. Magn. Mater.*, 2005, **285**, p 65–70
26. G.F. Zou, K. Xiong, C.L. Jiang, H. Li, T.W. Li, J. Du, and Y.T. Qian, Fe_3O_4 Nanocrystals with Novel Fractal, *J. Phys. Chem. B*, 2005, **109**, p 18356–18360
27. P.E. Lippens and M. Lannoo, Calculation of the Band Gap for Small CdS and ZnS Crystallites, *Phys. Rev. B*, 1989, **39**, p 10935–10942